第 35 卷第 8 期
2019 年 8 月

无 机 化 学 学 报
CHINESE JOURNAL OF INORGANIC CHEMISTRY

Vol.35 No.8
1509-1519

AuPd 和 AgPd 枝晶纳米催化剂催化甲酸分解制氢

刘 军 谢佳琦 吴新华 李 容 兰立新*
(湖南化工职业技术学院,制药与生物工程学院,株洲 412000)

摘要:由枝晶构成的 AuPd 和 AgPd 三维多孔泡沫薄膜在室温下分解甲酸制氢具有高催化活性。该高催化活性是由于纳米枝晶中存在大量的活性位点,如台阶、角、扭结、边缘以及合金间的电子效应。多孔泡沫膜除了具有较高的活性外,还具有其他优良的性能:在不需要有机添加剂的情况下,利用氢气泡模板法在 Ti 基板上可在 5 min 内快速沉积多孔泡沫催化剂,无需后处理便可用于催化甲酸分解制氢;通过将电沉积泡沫膜浸入或者拉出 HCOOH+HCOONa 溶液,可控制氢气的产生或停止;该泡沫催化剂通过去离子水清洗或者在 H_2SO_4 溶液中进行循环伏安扫描、干燥后就可活化重新使用。

关键词:物理化学;催化剂;电沉积;甲酸分解;制氢;枝晶
中图分类号:O643 **文献标识码**:A **文章编号**:1001-4861(2019)08-1509-11
DOI:10.11862/CJIC.2019.172

Hydrogen Production from Formic Acid Decomposition Using AuPd and AgPd Dendritic Nanocatalysts

LIU Jun XIE Jia-Qi WU Xin-Hua LI Rong LAN Li-Xin*
(*Department of Pharmaceutical and Biological Engineering, Hunan Chemical Vocational Technology College, Zhuzhou, Hunan* 412000, *China*)

Abstract: Three-dimensional (3D) porous thin films of AuPd and AgPd foams comprised of nanodendrites possess superior catalytic activity for the production of high-quality H_2 from formic acid decomposition at room temperature. The high catalytic activity was attributed to the presence of abundant active sites like steps, corners, kinks and edges in the nanodendrites, and to the electronic effect. Besides the high activity, there were some more advantages for the nanodendrtic alloy foam films. For example, the foam films could be quickly electrodeposited in 5 min on a Ti substrate utilizing the template of hydrogen bubbles without needing organic additives, and it could be used directly for the hydrogen production without post-treatments. The hydrogen production was easily controllable, and we could get hydrogen and stop hydrogen production just by immersing the electrodeposited foam film into and pulling it out of the solution of HCOOH+HCOONa. The foam films could also be easily reactivated either by drying after water cleaning or by potential cycling in H_2SO_4 solution.

Keywords: physicochemistry; catalyst; electrodeposition; formic acid decomposition; hydrogen production; dendrite

0 Introduction

Among various power sources, hydrogen energy is attracting increasing attention on account of its cleanness and sustainability[1]. However, storage and transfer of hydrogen gas are difficult with current technology because hydrogen gas is flammable and has a poor volumetric energy density. Noteworthily, formic acid has been considered as a promising in situ hydrogen source by catalytic decomposition[1-19] because it offers relatively high volumetric energy density, is non-toxic, can be safely handled in liquid and in aqueous solution,

收稿日期:2019-04-24。收修改稿日期:2019-05-22。
湖南省自然科学基金(No.2018JJ5021)资助项目。
*通信联系人。E-mail:1395561744@qq.com

and can be derived from hydrogenation of CO_2[20-21]. Decomposition of formic acid through two possible pathways is as follows[2,6]:

$$HCOOH \rightarrow H_2+CO_2 \quad (1)$$

$$HCOOH \rightarrow H_2O+CO \quad (2)$$

Reaction (**1**) is desired for hydrogen production and Reaction (**2**) should be avoided because CO is highly poisonous to catalysts. The content of carbon monoxide in hydrogen gas should be less than 10^{-3}% for direct use in fuel cells[2].

Recently, considerable progress has been made to obtain ultrapure hydrogen gas effectively from formic acid with different catalysts. For example, homogenous catalysts of metallic complexes (*e.g.* Ru and Fe complexes) showed excellent catalytic activities at ambient conditions towards the decomposition of formic acid in an inert atmosphere and in the presence of formate[10-11], amine[12-15] or in an organic solvent[16]. On the other hand, much more efforts have also been made recently in developing heterogenous catalysis of formic acid decomposition to surpass the efficiency by homogenous catalysis. Some nanocatalysts dispersed in aqueous solution of formic acid containing formate have also shown high activity for hydrogen production from decomposition of formic acid. Core-shell Ag@Pd/C nanoparticles[2], Pd/C catalysts[3], Pd-B-P/C[4], Au/ZrO_2 catalyst[5], Pd/C[6], TiO_2-supported AgPd@Pd nanocatalysts[9], AgPd nanoparticles[17], AuPd/C[18], and agglomerated Ag-Pd catalyst[22] are such representative nanocatalysts. However, further improvements of nanocatalysts in activity and selectivity are still requested to obtain high-quality hydrogen gas by decomposition of formic acid at room temperature.

As far as we knew, nanoporous alloy materials like AuPd[23], PdAg[24], PtNi[25], PtFe[26], PtCo[27], and PtRu[28-29] prepared by dealloying or hydrothermal method have also received considerable attention for electrocatalytic oxidation of small organic molecules. We first demonstrated that noble metal alloy foam materials of AuPt[30] with nanodendritic structures prepared by electrodeposition with a template of in situ produced hydrogen bubbles have high electrocatalytic activity for the oxidation of formic acid. Since the pioneer work on the electrodeposition of Cu and Sn foams[31], the hydrogen bubble dynamic template approach has been employed to prepare a lot of monometallic and bimetallic 3D porous foams, including Au [32-33], Ag [34-35], Ni [36], Bi [37], CuSn[38], PtPd[39], CuPd[40], Pt@Au_xCu_{100-x}[41], CoNi[42], and NiCu[43]. This is a very facile, fast and environment-friendly method for the preparation of metal foams without using protective reagents and additional template reagents.

In this work, we made detailed investigation for the first time on the preparation of nanodendritic AuPd and AgPd foam film catalysts with different atomic ratios by direct electrodeposition using hydrogen bubble dynamic templates and on their performance in hydrogen production from decomposition of formic acid at room temperature. These nanodendritic foam film catalysts show excellent activity for the decomposition of formic acid under room temperature and have great potential for practical applications in fuel cells.

1 Experimental

1.1 Reagents and materials

$HAuCl_4 \cdot 4H_2O$, $AgNO_3$, $Pd(C_2H_3O_2)_2$ and $PdCl_2$ were obtained from Sinopharm Chemical Reagent Co., Ltd. (Shanghai, China). A gold disk (1 mm diameter, purity 99.99%), a platinum foil (geometric area 1 cm^2) and Ti plates (geometric area 1 or 2 cm^2) were purchased from Tianjin Ai Da Heng Sheng Technology Development Co., Ltd. (Tianjin, China). Sulfuric acid (H_2SO_4), formic acid (HCOOH) and sodium formate (HCOONa) were purchased from the Factory of Hunan Normal University. All the chemicals were of analytical grade and were used as received. Milli-Q water with a resistivity of greater than 18 MΩ·cm was used in the preparation of aqueous solutions.

1.2 Electrodeposition of alloy foam films

In order to save Au and Pd precursors, exploratory electrodeposition of prous foams were performed firstly on a CHI 660C electrochemical workstation (Chenhua Instruments, Shanghai, China) with a small gold disk (1 mm diameter, purity 99.99%) or a Ti disk (2 mm diameter, purity 99.99%) purchased from Good Fellows as the substrate (working electrode). A platinum foil (geometric area 1 cm^2), and a saturated mercurous sulfate electrode (SMSE) were employed as the counter and reference electrode, respectively. Prior to use, the working electrode

was polished with 2 000 grit carbimet paper, followed by rinsing in Millipore water under ultrasonic waves. Then the electrode was electrochemically pretreated by cycling the potential between −0.7 and 1.1 V in 0.5 mol·L^{-1} H_2SO_4 at a scan rate of 100 mV·s^{-1} until a stable voltammogram was obtained. According to our previous experience for the electrodeposition of AuPt[30] alloy foams, electrodeposition of AuPd foam films were performed under a constant potential of −4 V for 300 s in a stationary solution of 2 mmol·L^{-1} $HAuCl_4$+0.58 mmol·L^{-1} $PdCl_2$+2 mol·L^{-1} H_2SO_4, 1 mmol·L^{-1} $HAuCl_4$+1 mmol·L^{-1} $PdCl_2$ +2 mol·L^{-1} H_2SO_4, 0.5 mmol·L^{-1} $HAuCl_4$ +1.5 mmol·L^{-1} $PdCl_2$+2 mol·L^{-1} H_2SO_4, and we denoted the deposited foam films as $Au_{100}Pd_{29}$, Au_1Pd_1, and Au_1Pd_3, respectively, according to the molar ratios of $HAuCl_4$/$PdCl_2$ in the feeding solution. For comparison, monometallic Au and Pd foam films were deposited in the same way by substituting the mixed precursors with 1 mmol·L^{-1} $HAuCl_4$ and 2 mmol·L^{-1} $PdCl_2$, respectively. AgPd foam films were also prepared by electrodeposition under −4 V for 300 s with precursor solutions of 1 mmol·L^{-1} $AgNO_3$+1 mmol·L^{-1} $Pd(C_2H_3O_2)_2$+2 mol·L^{-1} H_2SO_4.

An alternative two-step method was also employed to fabricate Pd-covered Au foams (denoted as Pd/Au). First, the gold foam was deposited under 4 V for 300 s in a solution of 2 mmol·L^{-1} $HAuCl_4$+2 mol·L^{-1} H_2SO_4, then, immersed in Milli-Q water for 10 min to remove the absorbed $AuCl_4^-$. Finally, the gold foam film electrode was transferred into a solution of 5 mmol·L^{-1} of $PdCl_2$+ 0.1 mol·L^{-1} $HClO_4$ to deposit Pd on the surface by galvanic replacement reaction for 45 min. The obtained Au/Pd bimetallic foam electrode was taken out and immersed into 100 mL Milli-Q water for 30 min to remove the absorbed precursor ions.

For convenience and practical applications, the alloy foam catalysts for the decomposition of formic acid were prepared with a direct current (DC) power (KXN-1550D) and a two-electrode configuration. A larger Ti plate (geometric area 2 cm^2) substrate and a platinum foil (geometric area 1 cm^2) were employed as the working and counter electrode, respectively. Prior to use, the Ti plates were polished with 2 000 grit carbimet paper, etched in 18%(*w*/*w*) HCl at 85 ℃ for 15 min to remove the surface oxide, and washed with Milli-Q water. Similar foam films can also be fabricated by electrodeposition under a constant voltage of 7 V for 200 s in different precursor solutions.

1.3 Determination of real surface areas

The real surface areas of these bimetallic and monometallic foam films were estimated from the double layer capacity measurement and the details of experiment and calculation were described in the Supplementary Information (Fig.S1, S2 and S3).

1.4 Characterization

The morphology images of the electrodeposited foam films were taken with a JEOL JSM-6360 scanning electron microscope (SEM) operating at 25 kV. TEM measurements were performed with JEOL-1230 electron microscope operating at a voltage 200 kV. Their bulk compositions were analyzed with an energy-dispersive X-rayspectrometer (EDS) using Tecnai 20. X-ray diffraction (XRD) analysis of the resulting products was carried out on a Dmax Rapid IIR diffractometer (Cu $K\alpha$ radiation (λ=0.154 2 nm)) in a scan range of 20°~120°, and the exposure time was 15 min at 40 kV and 40 mA.

1.5 Catalytic decomposition of formic acid and product analysis

The catalytic reactions of formic acid by the deposited foam films were performed at room temperature (~25 ℃) either in a test tube or in a beaker containing a solution of 6.64 mol·L^{-1} HCOOH and 3.32 mol·L^{-1} HCOONa. For anlalysis of gas chromatography (GC 5890F)[44], the produced gases were collected by the draining water method using a glass funnel and a gas-collecting bottle (35 mL) that were placed upside down. In addition, a graduated gas-collecting tube was used to record the gas volume released during 2 h. The deposited foam catalysts can be activated repeatedly after being washed with Milli-Q water and dried under an infrared lamp, or treated by potential cycling in 1 mol·L^{-1} H_2SO_4 within the range of −0.65 to 1 V at a scan rate of 100 mV·s^{-1}.

2 Results and discussion

2.1 Characterization of the electrodeposited AuPd foam films

The SEM images in Fig.1 show the porous structures of the prepared AuPd foam films with

different compositions by electrodeposition on Au disk electrodes (1 mm diameter) under a constant potential of −4 V for 300 s. The hierarchical pores in the forms were highly interconnected and look similar to each other (columns 1~2), resembling those of pure Au and pure Pd foams (Fig.S4). The pore size increased from bottom to top up to about 20 μm due to the coalescence of hydrogen gas bubbles during evolution from the substrate. The foams consisted of dense nanodendrites (column 3). Such dendritic AuPd alloy foams have larger surface area and provide more active sites like steps, corners, kinks and edges, which are beneficial to catalytic reactions[30]. Similar foam structures were obtained using either Ti disks (2 mm diameter) or Ti plates (geometric area 2 cm^2) under violent hydrogen evolution, which are given in Fig.S5 and S6. However, such foam structure was not observed (Fig.S7) while lessened the cathodic polarization extent from −4 to −0.8 V, where no severe hydrogen evolution occurred during electrodeposition.

The detailed dendritic structures of Au_1Pd_1 foams were further characterized by TEM and high-resolution TEM (HRTEM). As seen in Fig.2a and 2b, the dendrites were comprised of abundant nanocrystals sizing from 10 to 30 nm. Such morphology indicated that the formation of dendrites underwent orientated attachment of deposited nanocrystals [45-47]. The HRTEM image in Fig.2c reveals the atom lattice. The lattice fringe spacings of 0.234, 0.224 and 0.229 nm corresponded to the interplanar distance of Au (111), Pd (111) and AuPd (111) planes[48-49], respectively. In our experimental conditions, the Au_1Pd_1 foam film was rapidly electrodeposited in short duration.

The atomic compositions of AuPd foams were analyzed by EDS (Fig.3), which were roughly consistent with those of their corresponding precursor solutions (Table S1). It indicates that the foam composition could be controlled by the ratio of precursors.

In order to further determine the feature of bulk phase, the AuPd foam films were characterized by XRD.

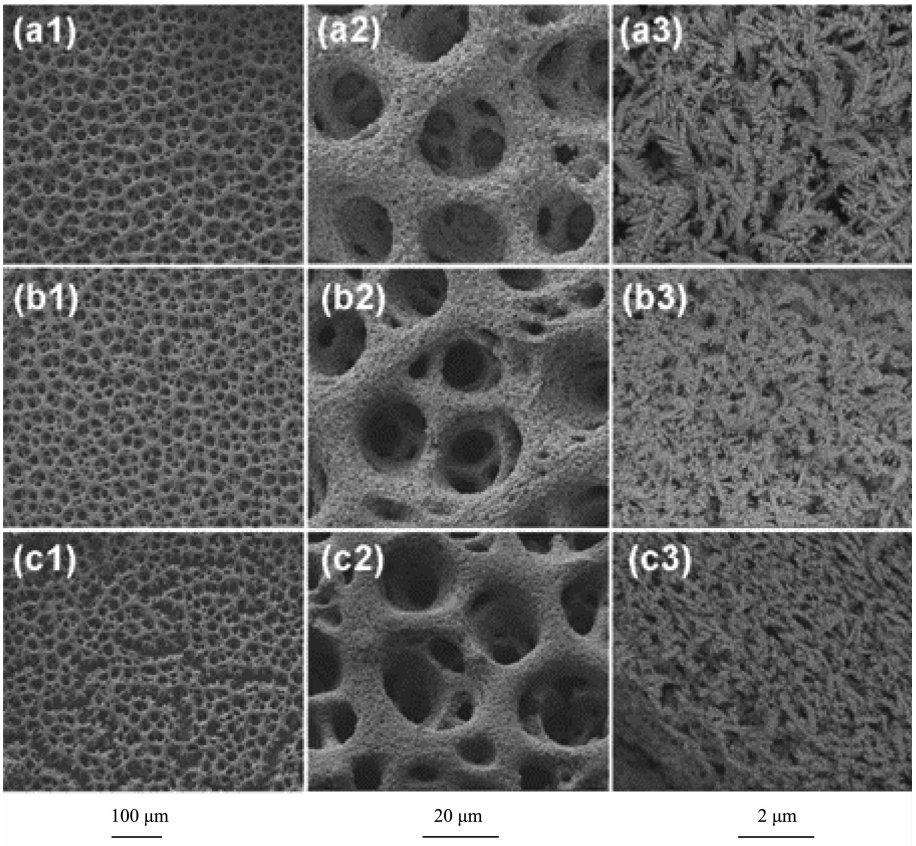

(a1~a3) 2 mmol·L^{-1} $HAuCl_4$+0.58 mmol·L^{-1} $PdCl_2$, (b1~b3) 1 mmol·L^{-1} $HAuCl_4$+1 mmol·L^{-1} $PdCl_2$ and (c1~c3) 0.5 mmol·L^{-1} $HAuCl_4$+1.5 mmol·L^{-1} $PdCl_2$

Fig.1 SEM images of 3D porous AuPd alloys electrodeposited on Au disk electrodes (1 mm diameter) at −4 V for 300 s in 2 mol·L^{-1} H_2SO_4 containing different Au/Pd ratios of precursor concentrations

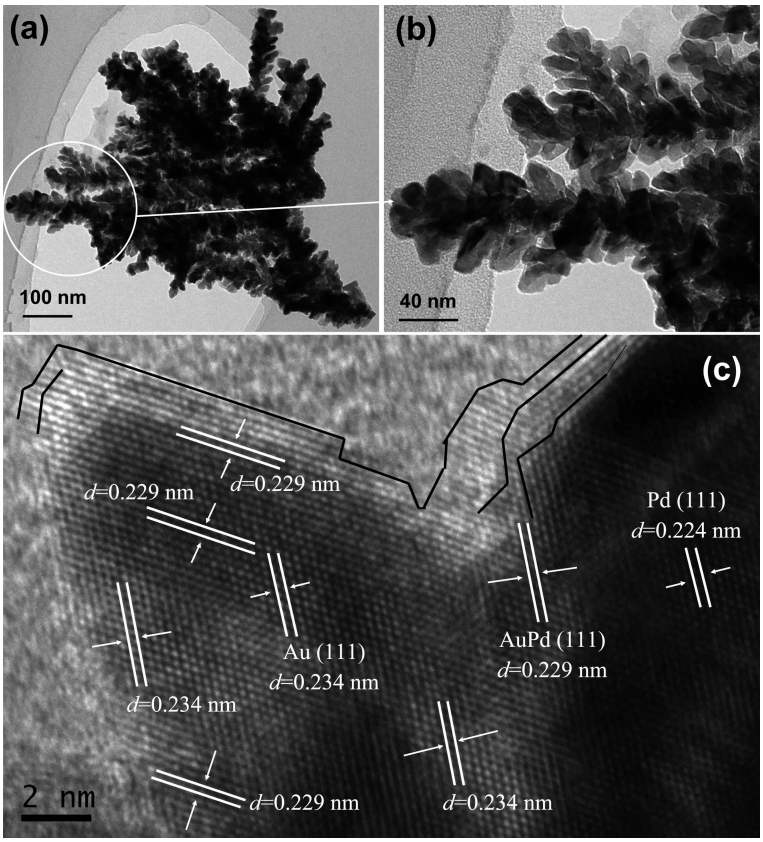

Fig.2　(a, b) TEM and (c) HRTEM images of the dendritic structure in the Au_1Pd_1 alloy foam

Fig.4 shows the XRD patterns of the deposited AuPd alloy foams as well as pure Pd and Au foams. The diffraction peaks at 38.23°, 44.34°, 64.63°,77.65° and 81.89° were assigned to Au (111), (200), (220), (311) and (222) planes, respectively, according to PDF No.04-0784 of Au; and the diffraction peaks at 40.09°, 46.47°, 68.26°, 82.33° and 86.88° were assigned to Pd (111), (200), (220), (311) and (222) planes, respectively, according to PDF No.46-1043 of Pd. The diffraction peaks of $Au_{100}Pd_{29}$, Au_1Pd_1 and Au_1Pd_3 samples fall well between those of pure Au and Pd, presenting a smooth transition from an Au-like pattern to a Pd-like pattern with the increase of Pd content. It suggests that the AuPd porous films are single-phase alloy nanomaterials. The detailed 2θ values of all samples are presented in Table S2.

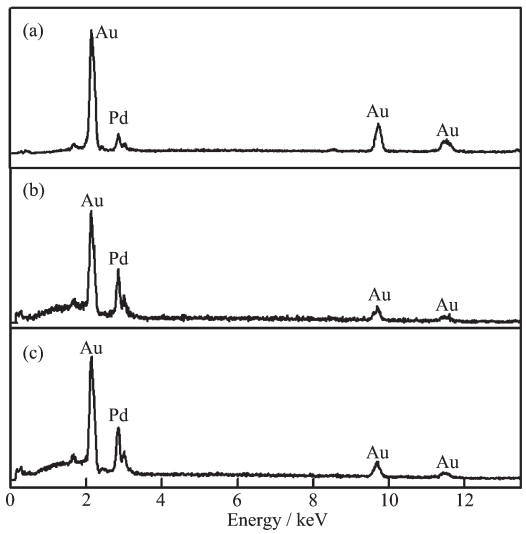

Fig.3　EDS spectra for the foam films of (a) $Au_{100}Pd_{29}$, (b) Au_1Pd_1 and (c) Au_1Pd_3

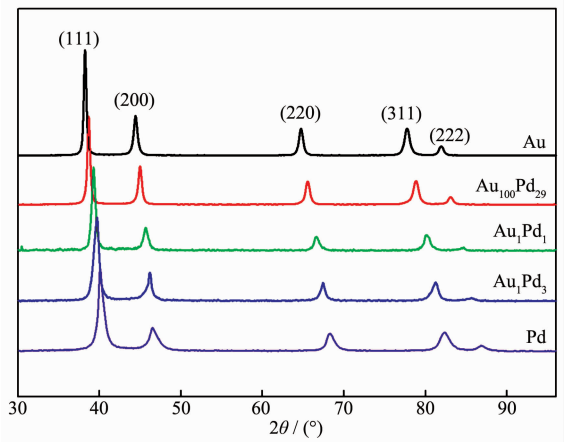

Fig.4　XRD patterns for foam films of pure Au, pure Pd and AuPd alloys

2.2 Hydrogen production from formic acid decomposition on the AuPd foam films

We found that the foam films of Au, Pd and AuPd alloys deposited on Au disk electrodes exhibited high catalytic activity in hydrogen generation from decomposition of formic acid at room temperature (~25 ℃). As demonstrated in Fig.5, vigorous gas released as soon as the foam film electrodes were immersed in the solution of 3.32 mol·L^{-1} HCOONa+6.64 mol·L^{-1} HCOOH. Among them, the Au_1Pd_1 foam film catalyst showed the highest reactive activity for the decomposition of formic acid. Similar phenomena were also observed on the foam films deposited on Ti disk electrodes (2 mm diameter) and on the Ti plate (geometric area 2 cm^2) for formic acid decomposition as shown in Fig.S8 and S9, respectively.

To produce more gas from formic acid decomposition, we used the larger Ti plate (geometric area 2 cm^2) as substrate to deposit foam films (Fig.S6 and S9(a~c)). Fig.6a shows the relationship between collected volume of reforming gas (H_2+CO_2) and collection time during 2 h with various porous film catalysts of Au, $Au_{100}Pd_{29}$, Au_1Pd_1, Au_1Pd_3 and Pd in 6.64 mol·L^{-1} HCOOH and 3.32 mol·L^{-1} HCOONa solution. To compare the catalytic activity of different metal foam films, the gas volume was scaled to unit active area, which was obtained by the method discribed in Fig.S1, S2 and S3. Apparently, Au_1Pd_1 foam film was the best catalyst among the five foam films, which gave a rather high maximum output of 169.8 mL·m^{-2} reforming gas in 2 h (It was 114.5 mL·m^{-2} in 2 h at 35 ℃, which could be calculated from the data in the reference[2] for Ag@Pd core-shell nanoparticles). Especially, the original reaction rate was extremely fast and about 48.09 mL·m^{-2} reforming gas was released in the first 1 min, being 28.31% of the total reforming gas in 120 min. The reaction rate then became steady after 20 min especially for the foam films of Au, Pd and $Au_{100}Pd_{29}$. The CO content in the reforming gas was determined to be 6.5×10^{-5} by gas chromatography (Fig.

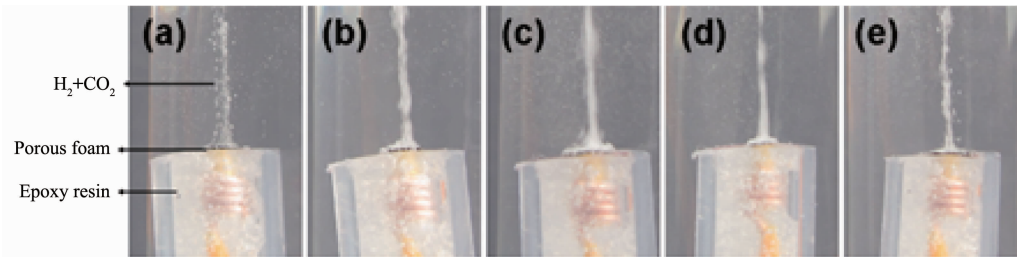

Fig.5 Photos for the hydrogen production at room temperature in 3.32 mol·L^{-1} HCOONa+6.64 mol·L^{-1} HCOOH from the decomposition of formic acid on the foam films of (a) Au, (b) $Au_{100}Pd_{29}$, (c) Au_1Pd_1, (d) Au_1Pd_3, and (e) Pd deposited on gold disk electrodes (1 mm diameter)

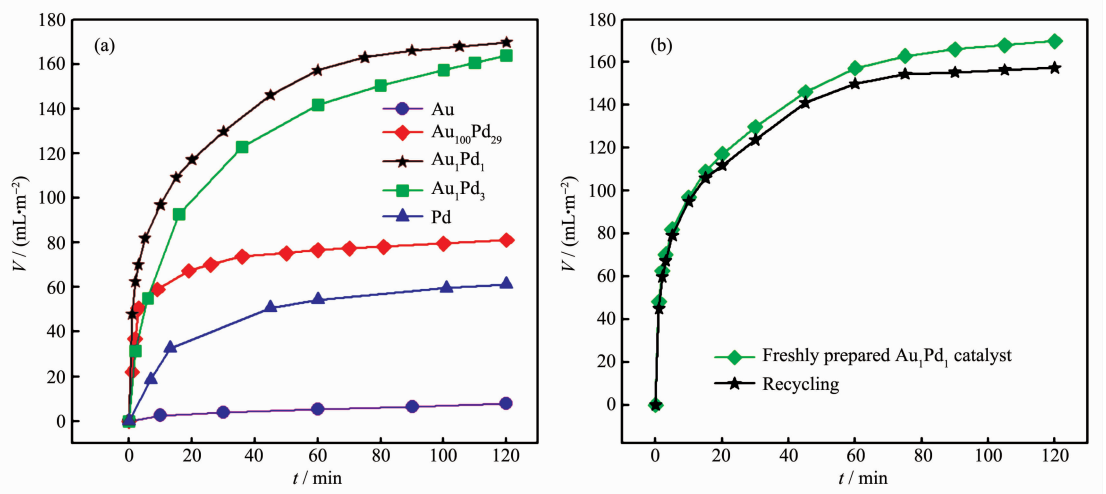

Fig.6 (a) Output volume of reforming gas (H_2+CO_2) during 120 min on the porous film catalysts of Au, $Au_{100}Pd_{29}$, Au_1Pd_1, Au_1Pd_3, and Pd in 6.64 mol·L^{-1} HCOOH+3.32 mol·L^{-1} HCOONa at room temperature (~25 ℃); (b) Cycling performance of the Au_1Pd_1 foam film

S10 and Table S3), which was rather low. Moreover, the content of CO_2 was detected to be 8.15% (less than 50%), which could be ascribed to the dissolution of CO_2 in view of the large volume of the HCOOH +HCOONa solution (2 L) we used to collect the gases conveniently. The turnover frequency (TOF)[2] during 2 h on Au_1Pd_1 alloy foam was up to 188 h^{-1}, which showed high catalytic activity towards the decomposition of formic acid at room temperature (~25 ℃).

The cumulation of CO at the foam film surface might be the reason for the decreased in decomposition rate of formic acid after 20 min. We found that the activity of the catalysts could be easily renewed by cleaning them in pure water and followed by drying in air under an infrared lamp for 2 h. During this treatment, the adsorbed CO was removed by oxygen species on the film surface resulted from the water and/or air. Fig.6b shows the results for repeated performances of the Au_1Pd_1 foam film catalyst in formic acid decomposition. After the cleaning and drying treatment, the catalytic activity of Au_1Pd_1 foam film was restored completely and the released gas volumes were almost the same for the two repeated performances, especially in the first 20 min.

The presence and removal of poisonous CO adsorbed on the AuPd foam films were confirmed by cyclic voltammograms in H_2SO_4 solution (Fig.S11). On the Au_1Pd_1 foam film without treatment by cleaning and drying there was a big sharp oxidation peak at 0.49 V in the first positive potential sweep, which is ascribed to the oxidation of adsorbed CO formed previously from the dissociative adsorption of formic acid. Meanwhile, hydrogen desorption peak vanished in the first positive potential sweep because the adsorbed CO inhibited the hydrogen adsorption. However, no such CO oxidative peak was observed for the Au_1Pd_1 foam film after cleaning and drying. It can also be seen that one potential cycle in 1 mol·L^{-1} H_2SO_4 solution could remove the adsorbed CO because hydrogen desorption peak around −0.5 V reappeared. This is another convenient way to reactivate the catalysts. The repeated performance of the Au_1Pd_1 foam film reactivated by potential cycles is shown in Fig.S12.

We also prepared Pd-covered Au (Pd/Au) foam films by galvanic displacement between Au foams and $PdCl_2$ solution because the Au nanodendrites were highly reactive. According to Chung and his co-workers, galvanic displacement of Au by Pt or Pd can only occur at places of active Au atoms[52], so the deposited Pd layer would be very thin. The Pd/Au foam film in Fig.S13 displayed similar morphology with that of AuPd alloy foam films (Fig.1). EDS analysis (Fig.S14) of the Pd/Au foam film showed that the average surface atomic ratio of Au to Pd was about 55.73∶44.27. However, the atomic ratio of Au to Pd varied from place to place because the active Au atoms on the dendritic Au foam film were not distributed uniformly.

A photo for the hydrogen production at room temperature from decomposition of formic acid on the Au/Pd foam film deposited on Ti plate was shown in Fig. S9d. The Pd/Au foam film catalyst possessed much higher activity for the formic acid decomposition (Fig.7) than pure foam films of Au and Pd (Fig.6a). 101.6, 7.89 and 61.40 mL·m^{-2} reforming gas were obtained in 2 h on the foam films of Pd/Au, pure Au and pure Pd, respectively. However, the performance of Pd-covered Au foam film towards formic acid decomposition was a little poor than that of Au_1Pd_1 alloy foam film (Fig.6a).

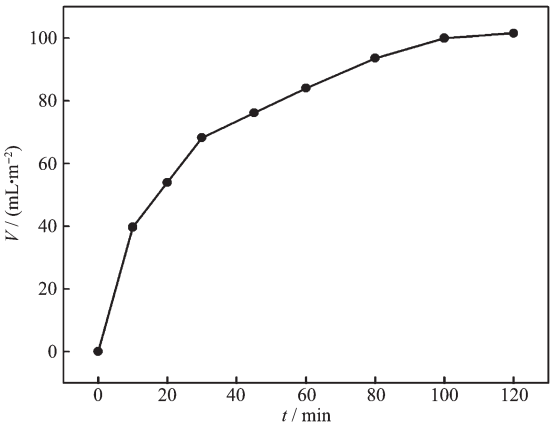

Fig.7　Output volume of reforming gas (H_2+CO_2) during 120 min with the Pd/Au foam film catalyst in 6.64 mol·L^{-1} HCOOH+3.32 mol·L^{-1} HCOONa at room temperature (~25 ℃)

2.3　Hydrogen production from formic acid decomposition on bimetallic AgPd foam films

We further deposited Ag_1Pd_1 foam film and investigated its catalytic activity for formic acid decomposition at room temperature (~25 ℃). Fig.8 shows

typical SEM images of the deposited Ag_1Pd_1 foam film. As can be clearly seen, the foam film have similar hierarchical porous structures, resembling that of AuPd foam films. Nevertheless, the wall of Ag_1Pd_1 foam (Fig. 8c) consisted of much smaller and thinner dendtrites than those of AuPd foams in Fig.1.

The representative TEM images in Fig.9 (a,b) demonstrated that the prepared nanodendritic AgPd foam film comprise of samll nanocrystals sizing from 10 to 20 nm. Such morphology also indicated that the formation of nanodendrites underwent orientated attachment of deposited nanocrystals[45-47]. Fig.9 (c) shows the HRTEM image of an AgPd sprout. The lattice fringe spacings of 0.224 and 0.232 nm corresponded to the interplanar distance of Pd (111) (PDF No.46-1043) and Ag (111) (PDF No.65-2871) planes, respectively. The orientations of the crystal planes suggested that the growth direction was along the [111] axis. On the other hand, we found that most of the lattice fringe spacings were assigned to Pd (111) plane on the surface of AgPd nanoparticles. The reason would be that galvanic replacement reaction took place between the freshly deposited Ag and Pd^{2+} ions in solution. This explantion was supported by EDS analysis shown in Fig.S15, where the atomic percentage of Pd in the AgPd foam was somewhat higher than that in the corresponding feeding solution.

The bulk phase of the AgPd foam film was characterized by XRD (Fig.10). The standard card of cubic Ag (PDF No.65-2871) and the XRD pattern of deposited pure Pd foam film are also shown in Fig.10 for comparison. The diffraction peaks of (111), (200), (220) and (311) planes both from pure Ag and from AgPd alloy appeared, suggesting that the Ag_1Pd_1 foam film was

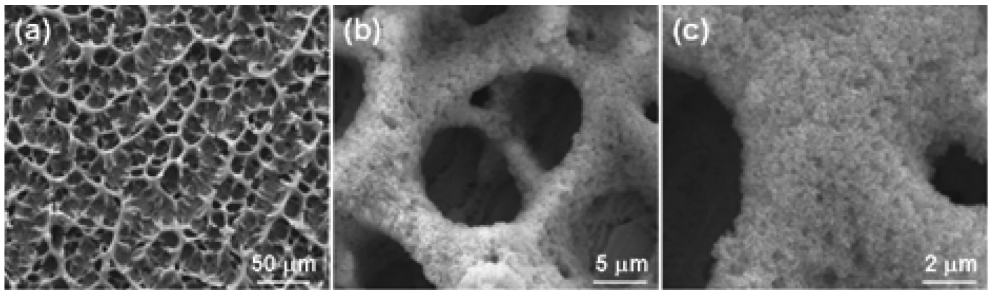

Fig.8 SEM images of 3D porous AgPd film electrodeposited on Au disk electrodes (1 mm diameter) at −4 V for 300 s in 2 mol·L^{-1} H_2SO_4 containing 1 mmol·L^{-1} $AgNO_3$+1 mmol·L^{-1} $Pd(CH_3COO)_2$

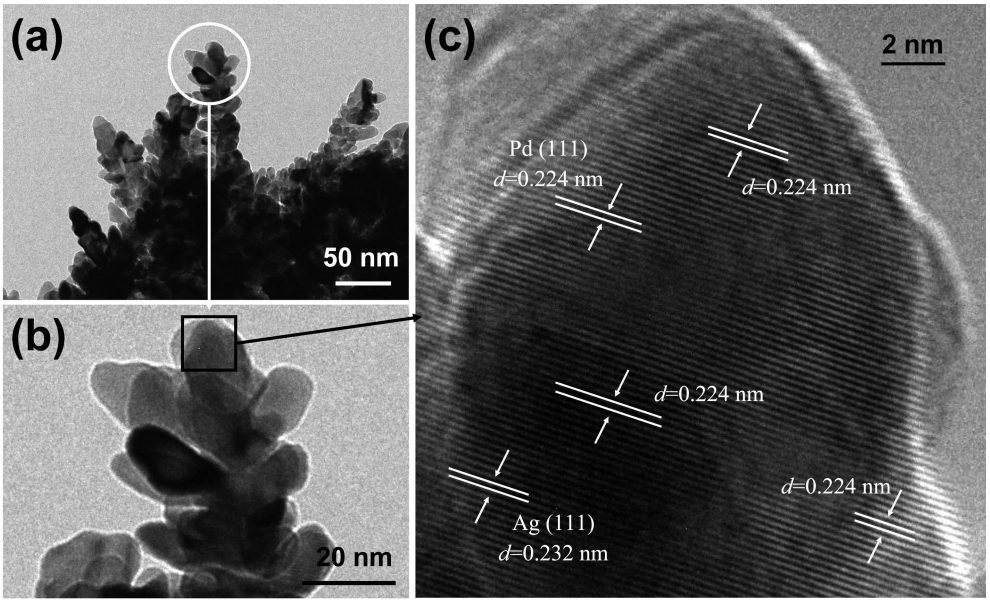

Fig.9 (a, b) TEM, and (c) HRTEM images of the dendritic structure in the Ag_1Pd_1 foam film electrodeposited in the solution of 1 mmol·L^{-1} $AgNO_3$+1 mmol·L^{-1} $Pd(CH_3COO)_2$+2 mol·L^{-1} H_2SO_4

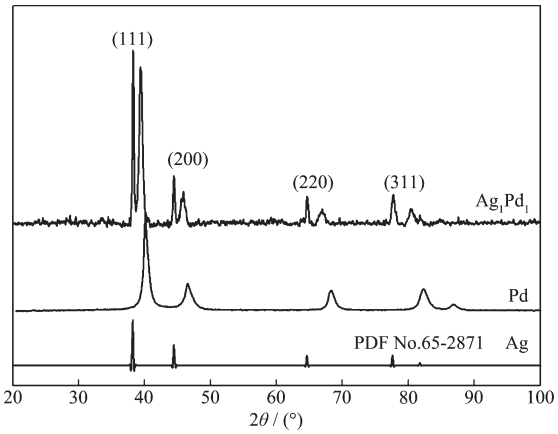

Fig.10　XRD patterns of foam films of Ag_1Pd_1 and pure Pd

a mixture of metallic Ag and AgPd alloy.

The Ag_1Pd_1 foam film also showed high catalytic activity toward the decomposition of formic acid at room temperature, which would be observed by naked eyes (Fig.S16). Fig.11 gives the relationship between released gas volume and collection time. The original reaction rate on the Ag_1Pd_1 foam was rather fast and about 128.2 $mL \cdot m^{-2}$ reforming gas was released in the first 8 min and gave a maximum output of 279.5 $mL \cdot m^{-2}$ reforming gas in 2 h, which was more than that on the Au_1Pd_1 foam film catalyst due to the electronic effect[2]. Comparison of catalytic activities of AuPd, AgPd foams and different nano-power catalysts for hydrogen generation from formic acid were showed in Table 1. Among all the catalysts tested, Ag_1Pd_1 foam exhibited the high catalytic activity with the TOF value of 308 h^{-1} at room temperature toward hydrogen generation from formic acid, which is higher than of most previously reported values.

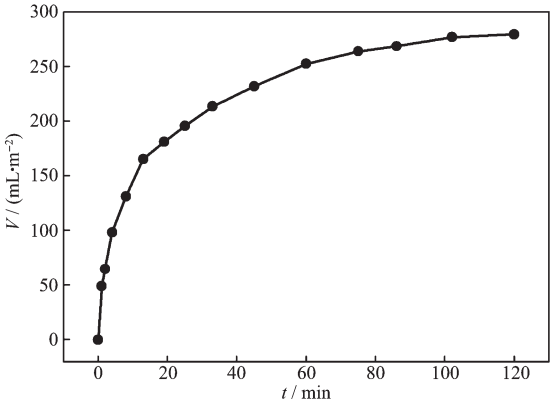

Fig.11　Output volume of reforming gas (H_2+CO_2) during 120 min for the foam film catalyst of Ag_1Pd_1 in 6.64 $mol \cdot L^{-1}$ HCOOH+3.32 $mol \cdot L^{-1}$ HCOONa solution at room temperature (~25 ℃)

Table 1　Comparison of activities of different catalysts for hydrogen generation from formic acid

Catalyst	Reaction condition	TOF / h^{-1}	T / K	Reference
Au_1Pd_1 foam	HCOOH+HCOONa	188	298	This work
Ag_1Pd_1 foam	HCOOH+HCOONa	308	298	This work
Ag@Pd (1:1)	HCOOH	125	293	[2]
Ag@Pd (1:1)	HCOOH	156	308	[2]
Ag@Pd (1:1)	HCOOH	252	323	[2]
Ag/Pd alloy (1:1)	HCOOH	144	293	[2]
Pd (2.3 nm)	HCOOH	24	293	[2]
Pd (3.2 nm)	HCOOH	25	293	[2]
Ag@Pd/C (1:1)	HCOOH	192	293	[2]
Pd@SiO_2	HCOOH+HCOONa	70	365	[3]
Pd-B-P/C	HCOOH+HCOONa	798	303	[4]
Au/ZrO_2	HCOOH+dimethylethanolamine	1 166	333	[5]
Pd/C	HCOOH+HCOONa	565	303	[6]
PdNiAg/C	HCOOH+HCOONa	85	323	[9]
Ag_1Pd_3/N-G	HCOOH+HCOONa	309.1	298	[17]
Au-Pd/N-C	HCOOH	2 221	323	[18]

3　Conclusions

To conclude, we have provided a facile and green way to prepare AuPd and AgPd foam film catalysts composed of special porous structures with nanodendritic walls. Among the prepared AuPd dendritic foam film catalysts, the foam of Au_1Pd_1 displayed the highest catalytic activity for the decomposition of formic

acid at room temperature, and the foam of Ag_1Pd_1 was better than Au_1Pd_1. The high catalytic activity of the dendritic foam films of Au_1Pd_1 and Ag_1Pd_1 is attributed to the presence of abundant active sites like steps, corners, kinks and edges in the nanodendrites, and to the electronic effect. Such supported thin films of nanocatalysts are easier to operate than that of dispersed nanoparticles and homogeneous catalysts because they are convenient for controlling, seperating and recycling. We hope that this work opens a new avenue to develop supported solid film nanocatalysts for hydrogen production from formic acid decomposition in aqueous solution.

Supporting information is available at http://www.wjhxxb.cn

References:

[1] Wang X, Meng Q L, Gao L Q, et al. *Int. J. Hydrogen Energy*, **2018**,**43**:7055-7071

[2] Tedsree K, Li T, Jones S, et al. *Nat. Nanotechnol.*, **2011**,**6**:302-307

[3] Yadav M, Singh A K, Tsumori N, et al. *J. Mater. Chem.*, **2012**,**22**:19146-19150

[4] CHEN Tao(陈涛), ZHANG Lai-Ying(张来英), ZHANG Hong-Bin(张鸿斌), et al. *Journal of Xiamen University*: *Natural Science*(厦门大学学报:自然科学版), **2017**,**56**(6):817-822

[5] Bi Q Y, Lin J D, Liu Y M, et al. *Int. J. Hydrogen Energy*, **2016**,**41**:21193-21202

[6] JIAO Xiao-Xin(焦晓新), ZHANG Xiao-Xiao(郑潇潇), ZHANG Hong-Bin(张鸿斌). *Journal of Xiamen University*: *Natural Science*(厦门大学学报:自然科学版), **2015**,**54**(5):707-712

[7] Gazsi A, Bnsgi T, Solymosi F. *J. Phys. Chem. C*, **2011**,**115**:15459-15466

[8] Manuel O, Lglesia E. *Angew. Chem. Int. Ed.*, **2009**,**48**:4800-4803

[9] Yurderi M, Bulut A, Zahmakiran M, et al. *Appl. Catal. B*, **2014**,**160**:514-524

[10]Fellay C, Dyson P J, Laurenczy G. *Angew. Chem. Int. Ed.*, **2008**,**47**:3966-3968

[11]Czaun M, Goeppert A, May R, et al. *ChemSusChem*, **2011**,**4**:1241-1248

[12]Boddien A, Loges B, Junge H, et al. *ChemSusChem*, **2008**,**1**:751-758

[13]Loges B, Boddien A, Junge H, et al. *Angew. Chem. Int. Ed.*, **2008**,**47**:3962-3965

[14]Junge H, Boddien A, Capitta F, et al. *Tetrahedron Lett.*, **2009**,**50**:1603-1606

[15]Boddien A, Loges B, Grtner F, et al. *J. Am. Chem. Soc.*, **2010**,**132**:8924-8934

[16]Boddien A, Mellmann D, Grtner F, et al. *Science*, **2011**,**333**:1733-1736

[17]DU Cheng(杜成), HEI Ze-Xiu(黑秀泽), LUO Wei(罗威), et al. *Scientia Sinica*: *Chimica*(中国科学:化学), **2016**,**46**(5):487-495

[18]CHEN Yang(陈旸), GAO Ling-Feng(高凌峰), QIU Zhen(邱镇). *Industrial Catalysis*(工业催化), **2016**,**24**(7):27-31

[19]Grasemann M, Laurenczy G. *Energy Environ. Sci.*, **2012**,**5**:8171-8181

[20]Enthaler S, Langermann J V, Schmidt T. *Energy Environ. Sci.*, **2010**,**3**:1207-1217

[21]Maenaka Y, Suenobu T, Fukuzumi S. *Energy Environ. Sci.*, **2012**,**5**:7360-7367

[22]Liu J, Lan L X, Li R, et al. *Int. J. Hydrogen Energy*, **2016**, **41**:951-958

[23]Lang X Y, Guo H, Chen L Y, et al. *J. Phys. Chem. C*, **2010**, **114**:2600-2603

[24]Chen S, Adams B D, Chen A C. *Electrochim. Acta*, **2010**,**56**:61-67

[25]Chen S, Wu S, Zheng J F, et al. *J. Electroanal. Chem.*, **2009**,**628**:55-59

[26]Qiu H J, Huang X R. *J. Mater. Chem.*, **2012**,**22**:7602-7608

[27]Qiu H J, Zou F X. *ACS Appl. Mater. Interfaces*, **2012**,**4**:1404-1410

[28]Koczkur K, Yi Q F, Chen A C. *Adv. Mater.*, **2007**,**19**:2648-2652

[29]Xu C X, Wang L, Mu X L, et al. *Langmuir*, **2010**,**26**:7437-7443

[30]Liu J, Cao L, Huang W, et al. *ACS Appl. Mater. Interfaces*, **2011**,**3**:3552-3558

[31]Shin H C, Dong J, Liu M L. *Adv. Mater.*, **2003**,**15**:1610-1614

[32]Cherevko S, Chung C H. *Electrochim. Acta*, **2011**,**13**:16-19

[33]LIU Jun(刘军), LI Rong(李容), XIAO Jie(肖洁), et al. *Chinese J. Inorg. Chem.*(无机化学学报), **2018**,**34**(6):1166-1172

[34]Cherevko S, Chung C H. *Electrochim. Acta*, **2010**,**55**:6383-6390

[35]Cherevko S, Xing X L, Chung C H. *Electrochem. Commun.*, **2010**,**12**:467-470

[36]NIU Zhen-Jiang(牛振江), SUN Ya-Feng(孙雅峰), CHEN Die(陈蝶), et al. *Chinese J. Inorg. Chem.*(无机化学学报), **2006**,**22**(5):930-934

[37]CHEN Xin(陈欣), CHEN Shu(陈述), HUANG Wei(黄炜), et al. *Journal of Materials Engineering*(材料工程), **2008**,**10**:243-246

[38]Shin H C, Liu M L. *Adv. Funct. Mater.*, **2005**,**15**:582-586
[39]Liu J, Cao L, Huang W, et al. *J. Electroanal. Chem.*, **2012**, **686**:38-45
[40]Najdovski I, Selvakannan P R, OMullane A P, et al. *Chem. Eur. J.*, **2011**,**17**:10058-10063
[41]Cherevko S, Kulyk N, Chung C H. *Langmuir*, **2012**,**28**:3306-3315
[42]Rafailovi L D, Gammer C, Rentenberger C, et al. *Phys. Chem. Chem. Phys.*, **2012**,**14**:972-980
[43]Choi W S, Jung H R, Kwon S H, et al. *J. Mater. Chem.*, **2012**,**22**:1028-1032
[44]King R B, Bhattacharyya N K, Wiemers K D. *Environ. Sci. Technol.*, **1996**,**30**:1292-1299
[45]Guo C, Xia Y, Xu Y Z, et al. *Mater. Lett.*, **2011**,**65**:2326-2329
[46]Liu J, Fu Y Y, Guo A, et al. *J. Phys. Chem. C*, **2008**,**112**:4242-4247
[47]Witten T A, Sander L M. *Phys. Rev. Lett.*, **1981**,**47**:1400-1403
[48]Zhang G R, Zhao D, Feng Y Y, et al. *ACS Nano*, **2012**,**6**:2226-2236
[49]Lee Y W, Kim M J, Kim Y N, et al. *J. Phys. Chem. C*, **2010**,**114**:7689-7693
[50]Patra S, Viswanath B, Barai K, et al. *ACS Appl. Mater. Interfaces*, **2010**,**2**:2965-2969
[51]Zhang L, Zhang J W, Kuang Q, et al. *J. Am. Chem. Soc.*, **2011**,**133**:17114-17117
[52]Cherevko S, Kulyk N, Chung C H. *Electrochim. Acta*, **2012**, **69**:190-196